INTERNATIONAL JOURNAL FOR NUMERICAL METHODS IN FLUIDS
Int. J. Numer. Meth. Fluids 2002; **39**:939–959 (DOI: 10.1002/fld.353)

A finite volume approach for unsteady viscoelastic fluid flows

Hassan Al Moatassime[1,*,†] and Driss Esselaoui[2]

[1] *Université Cadi Ayyad, Faculté des Sciences et Techniques, avenue Abdelkrim Khattabi, B.P. 618 Guéliz Marrakech, Morocco*
[2] *Laboratoire des Sciences de l'Ingénieur, Analyse Numérique et Optimisation, Université Ibn Tofail, Kénitra, Morocco*

SUMMARY

A finite volume, time-marching for solving time-dependent viscoelastic flow in two space dimensions for Oldroyd-B and Phan Thien–Tanner fluids, is presented. A non-uniform staggered grid system is used. The conservation and constitutive equations are solved using the finite volume method with an upwind scheme for the viscoelastic stresses and an hybrid scheme for the velocities. To calculate the pressure field, the semi-implicit method for the pressure linked equation revised method is used. The discretized equations are solved sequentially, using the tridiagonal matrix algorithm solver with under-relaxation. In both, the full approximation storage multigrid algorithm is used to speed up the convergence rate. Simulations of viscoelastic flows in four-to-one abrupt plane contraction are carried out. We will study the behaviour at the entrance corner of the four-to-one planar abrupt contraction. Using this solver, we show convergence up to a Weissenberg number *We* of 20 for the Oldroyd-B model. No limiting Weissenberg number is observed even though a Phan Thien–Tanner model is used. Several numerical results are presented. Smooth and stable solutions are obtained for high Weissenberg number. Copyright © 2002 John Wiley & Sons, Ltd.

KEY WORDS: finite volume method; viscoelastic; staggered grid; FAS algorithm; SIMPLER algorithm; TDMA solver; Oldroyd-B model; Phan Thien–Tanner model; planar four-to-one contraction

1. INTRODUCTION

Polymeric fluids are of particular interest in the numerical simulation community because of the rich variety of behaviour observed in experiments. Several families of constitutive equations exist, including integral-type equations and differential models [1].

Flows through contractions have been of primary importance. These problems manifest sufficiently complex flow phenomena. They provide a challenge to the numerical algorithms. A major problem afflicting the early numerical techniques was the failure to obtain solutions at Weissenberg numbers much greater than unity. This phenomena is called 'the high

* Correspondence to: H. Al-Moatassime, Université Cadi Ayyad, Faculté des Sciences et Techniques, avenue Abdelkrim Khaltabi, B.P. 618, Gueliz, 4000 Marrakech, Morocco.
† E-mail: hassan.al-moatassime@fstg-marrakech.ac.ma

Received June 2001
Revised December 2001

Weissenberg number problem' (see Chapter 11 in References [2, 3]). The cause of the failure of these numerical simulations is purely numerical: the mixed elliptic–hyperbolic type of the equations, geometrical singularities (corner of the abrupt contraction). Theoretical work [4, 5] has made it possible to propose robust and efficient numerical schemes.

During the last few years, remarkable progress has been achieved in numerical simulations. Many numerically stable and accurate algorithms for computing some viscoelastic flows have been proposed, among these are the 4×4 mixed element of Crochet and Marchal [6], the explicitly elliptic momentum equation (EEME) method of King *et al.* [7] and the elastic–viscous split stress (EVSS) method of Rajagopalan *et al.* [8]. Convergence of each method of the calculations with mesh refinement was demonstrated. Marchal and Crochet were able to solve the axisymmetric 4:1 contraction problem for essentially unlimited Deborah numbers for an Oldroyd-B fluid. They report solutions for Deborah numbers as high as 64. Rao and Finlayson [9] applied the EEME to the axisymmetric 4:1 contraction problem and found that the use of EEME resulted in better solutions than could be obtained by solving the Cauchy momentum equation when quadratic polynomials are used to approximate the stress field on each element. They also employed an adaptive mesh technique to refine the mesh in regions where the residual was high. The highest Deborah number for which solutions could be obtained was 3.84. Rao and Finlayson [10] have used the EEME and the inconsistent streamline upwind Petrov–Galerkin method in conjunction with finite element spaces that are biquadratic velocity, bilinear pressure and bicubic stress field on quadrilaterals. The highest Deborah number for which calculations were successful was 19.2 for a Maxwell fluid and 42 for an Oldroyd-B fluid. Fortin and Fortin [11] have simulated the flow through the four-to-one abrupt plane contraction of an Oldroyd-B fluid by using the streamline upwind (SU) technique and Lesaint–Raviart method and they obtained solutions at high Weissenberg number. Fortin and Fortin [12] proposed an iterative method based on the generalized minimal residual (GMRES) method, they could obtain solutions for Deborah number as high as 4.5 for the stick-slip problem. Later Fortin and Zine [13] redefined an extra-stress tensor and improved the range of convergence, the critical Deborah number was increased to 16 for the same problem but still lower than the limit achieved by Marchal and Crochet [6]. Beris *et al.* [14] developed a combined pseudo-spectral/finite element method to simulate the flow of a Maxwell fluid between eccentrically rotating cylinders.

Simulations based on the finite difference method are also used in the computation of viscoelastic fluid flow [15–19]. Al Moatassime and Jouron [20] solved the four-to-one abrupt plane contraction and the stick-slip problems by using the fall approximation storage (FAS) multigrid method. A critical Weissenberg number was found when the Oldroyd-B model was used and this number decreases upon mesh refinement. The highest Weissenberg number for which calculations were successful was $We=10.0$ for the stick-slip problem and $We=6.0$ for the flow through four-to-one abrupt plane contraction. For the PTT model, calculation is pursued up to $We=15.0$ for the four-to-one contraction problem and none limiting value of Weissenberg has been reached for the stick-slip problem. Al Moatassime and Esselaoui [21] have proposed a FAS algorithm and a cell by cell relaxation procedure to solve the steady stick-slip and the flow through four-to-one abrupt plane contraction problems. For the stick-slip problem they could obtain solutions for We as high as 14 and the highest We for the four-to-one abrupt plane contraction problem was 12.

The finite volume method is gradually been used more within the viscoelastic context (see References [22–27]).

An outline of this paper is as follows. In Section 2 we introduce the problem definition. The next section is devoted to the description of the finite volume method. Then we present numerical results of flows in four-to-one abrupt plane contraction that will exhibit some of the interesting properties of viscoelastic fluids. We draw conclusion in Section 7.

2. BASIC FLOW EQUATIONS

2.1. Governing equations

We shall consider the unsteady, incompressible and isothermal flow of a viscoelastic fluid. The equation of continuity and the equation of motion can be reduced into the dimensionless form as follows:

$$\nabla U = 0 \tag{1}$$

$$Re\,\frac{\partial U}{\partial t} + Re(U\cdot\nabla)U = \nabla\underline{\underline{\sigma}} \tag{2}$$

$$\underline{\underline{\sigma}} = -P.\underline{\underline{I}} + 2(1-\omega_r)\underline{\underline{D}} + \underline{\underline{\tau}} \tag{3}$$

Here P represents the dimensionless pressure; U represents the dimensionless velocity vector; $\underline{\underline{I}}$ is a unit tensor; $\underline{\underline{\tau}}$ and $\underline{\underline{\sigma}}$ represent the dimensionless stress and total stress tensor, respectively; $Re = \rho U_\mathrm{t} L_\mathrm{t}/\eta$ is the Reynolds number, where ρ is the density of the fluid; η is the field viscosity; L_t and U_t are a typical length and a typical velocity of the flow, respectively.

Our choice of constitutive models are those due to Phan Thien–Tanner [28, 29] and Oldroyd-B. The following equation should exist:

$$\left(1 + \varepsilon\,\frac{We}{\omega_r}\,\mathrm{Tr}(\underline{\underline{\tau}})\right)\underline{\underline{\tau}} + We\,\frac{\mathrm{D}_a\underline{\underline{\tau}}}{\mathrm{D}_a t} = 2\omega_r\underline{\underline{D}} \tag{4}$$

The operator $\mathrm{D}_a/\mathrm{D}_t$ is the objective time derivative defined by

$$\frac{\mathrm{D}_a\underline{\underline{\tau}}}{\mathrm{D}t} = \left(\frac{\partial}{\partial t} + \underline{U}\cdot\nabla\right)\underline{\underline{\tau}} + \underline{\underline{\tau}}\,\underline{\underline{W}} - \underline{\underline{\tau}}\,\underline{\underline{W}} - a(\underline{\underline{D}}\,\underline{\underline{\tau}} - \underline{\underline{\tau}}\,\underline{\underline{D}})$$

where $\underline{\underline{D}}$ is the strain rate tensor $\underline{\underline{D}} = \frac{1}{2}(\nabla\underline{U} + (\nabla\underline{U})^\mathrm{T})$; $\underline{\underline{W}}$ is the vorticity tensor; $\underline{\underline{W}} = \frac{1}{2}(\nabla\underline{U} - (\nabla\underline{U})^\mathrm{T})$, the parameter a satisfies $-1 \leqslant a \leqslant 1$, $We = \lambda_1\,U/L$ is the Weissenberg number (λ_1 is relaxation time) and $\omega_r = 1 - \lambda_2/\lambda_1$ (λ_2 is retardation time).

The Oldroyd-B model is obtained by setting $\varepsilon = 0$.

For a two-dimensional system, the dimensionless unsteady state problem can be written as

$$\frac{\partial U}{\partial x} + \frac{\partial V}{\partial y} = 0$$

$$\begin{aligned} &Re\,\frac{\partial U}{\partial t} + \frac{\partial}{\partial x}\left(Re\,U\,U - (1-\omega_r)\,\frac{\partial U}{\partial x}\right) + \frac{\partial}{\partial y}\left(Re\,V\,U - (1-\omega_r)\,\frac{\partial U}{\partial y}\right) \\ &\quad = -\frac{\partial P}{\partial x} + \frac{\partial \tau_{xx}}{\partial x} + \frac{\partial \tau_{xy}}{\partial y} \end{aligned}$$

$$Re\,\frac{\partial V}{\partial t}+\frac{\partial}{\partial x}\left(Re\,U\,V-(1-\omega_r)\,\frac{\partial V}{\partial x}\right)+\frac{\partial}{\partial y}\left(Re\,V\,V-(1-\omega_r)\,\frac{\partial V}{\partial y}\right)$$
$$=-\frac{\partial P}{\partial y}+\frac{\partial\tau_{yy}}{\partial y}+\frac{\partial\tau_{xy}}{\partial x}$$

$$\left(1+\varepsilon\,\frac{We}{\omega_r}\,\mathrm{Tr}(\underline{\underline{\tau}})\right)\tau_{xx}+We\,\frac{\partial\tau_{xx}}{\partial t}+\frac{\partial}{\partial x}(We\,U\,\tau_{xx})+\frac{\partial}{\partial y}(We\,V\,\tau_{xx})$$
$$=2w_r\,\frac{\partial U}{\partial x}+2\,a\,We\,\frac{\partial U}{\partial x}\,\tau_{xx}+a\,We\left(\frac{\partial U}{\partial y}+\frac{\partial V}{\partial x}\right)\tau_{xy}+We\left(\frac{\partial U}{\partial y}-\frac{\partial V}{\partial x}\right)\tau_{xy}$$

$$\left(1+\varepsilon\,\frac{We}{\omega_r}\,\mathrm{Tr}(\underline{\underline{\tau}})\right)\tau_{yy}+We\,\frac{\partial\tau_{yy}}{\partial t}+\frac{\partial}{\partial x}(We\,U\,\tau_{yy})+\frac{\partial}{\partial y}(We\,V\,\tau_{yy})$$
$$=2w_r\,\frac{\partial V}{\partial y}+2\,a\,We\,\frac{\partial V}{\partial y}\,\tau_{yy}+a\,We\left(\frac{\partial U}{\partial y}+\frac{\partial V}{\partial x}\right)\tau_{xy}+We\left(\frac{\partial V}{\partial x}-\frac{\partial U}{\partial y}\right)\tau_{xy}$$

$$\left(1+\varepsilon\,\frac{We}{\omega_r}\,\mathrm{Tr}(\underline{\underline{\tau}})\right)\tau_{xy}+We\,\frac{\partial\tau_{xy}}{\partial t}+\frac{\partial}{\partial x}(We\,U\,\tau_{xy})+\frac{\partial}{\partial y}(We\,V\,\tau_{xy})$$
$$=w_r\left(\frac{\partial U}{\partial y}+\frac{\partial V}{\partial x}\right)-\frac{1}{2}\,We(\tau_{xx}-\tau_{yy})\left(\frac{\partial U}{\partial y}-\frac{\partial V}{\partial x}\right)+\frac{1}{2}\,a\,We(\tau_{xx}+\tau_{yy})\left(\frac{\partial U}{\partial y}+\frac{\partial V}{\partial x}\right)$$

where U and V are the velocity components, respectively, in the x and y directions;

$$\underline{\underline{\tau}}=\begin{pmatrix}\tau_{xx} & \tau_{xy}\\ \tau_{xy} & \tau_{yy}\end{pmatrix}$$

The system above is solved with appropriate initial conditions $\underline{U}(\cdot,t)=\underline{U}^0(\cdot),\underline{\underline{\tau}}(\cdot,t)=\underline{\underline{\tau}}^0(\cdot)$, $P(\cdot,t)=P^0(\cdot)$ and boundary conditions.

The problem can be symbolized by

$$\text{find } (U,P.\underline{\underline{\tau}}) \text{ solution of } L(U,P,\underline{\underline{\tau}})=0 \text{ in } \Omega \tag{5}$$

where L is a non-linear operator.

3. NUMERICAL METHOD

All of the governing equations can be written in the form of the general transport equation as follows:

$$\frac{\partial}{\partial t}(\wedge\,\Phi)+\frac{\partial}{\partial x}\left(\wedge\,U\,\Phi-\Gamma\,\frac{\partial\Phi}{\partial x}\right)+\frac{\partial}{\partial y}\left(\wedge\,V\,\Phi-\Gamma\,\frac{\partial\Phi}{\partial y}\right)=S_\Phi \tag{6}$$

where Φ is the primitive working variable, the coefficients Γ and $\wedge$ have different meanings for different working variables, and S_Φ represents the source term which includes all the terms that cannot be accommodated in the convective and diffusion terms and has different context

Table I. The definition of different variables.

Φ	$\wedge$	Γ	S_Φ
1	1	0	0
U	Re	$1-w_r$	$-\dfrac{\partial P}{\partial x}+\dfrac{\partial \tau_{xx}}{\partial x}+\dfrac{\partial \tau_{xy}}{\partial y}$
V	R	$1-w_r$	$-\dfrac{\partial P}{\partial y}+\dfrac{\partial \tau_{yy}}{\partial y}+\dfrac{\partial \tau_{xy}}{\partial x}$
τ_{xx}	We	0	$We\left(\dfrac{\partial U}{\partial y}-\dfrac{\partial V}{\partial x}\right)\tau_{xy}+2aWe\,\dfrac{\partial U}{\partial x}\,\tau_{xx}$ $+a\,We\left(\dfrac{\partial U}{\partial y}+\dfrac{\partial V}{\partial x}\right)\tau_{xy}+2w_r\,\dfrac{\partial U}{\partial x}-\left(1+\varepsilon\,\dfrac{We}{\omega_r}\,\mathrm{Tr}(\underline{\underline{\tau}})\right)\tau_{xx}$
τ_{yy}	We	0	$-We\left(\dfrac{\partial U}{\partial y}-\dfrac{\partial V}{\partial x}\right)\tau_{xy}+2\,a\,We\,\dfrac{\partial V}{\partial y}\,\tau_{yy}$ $+a\,We\left(\dfrac{\partial U}{\partial y}+\dfrac{\partial V}{\partial x}\right)\tau_{xy}+2w_r\,\dfrac{\partial V}{\partial y}-\left(1+\varepsilon\,\dfrac{We}{\omega_r}\,\mathrm{Tr}(\underline{\underline{\tau}})\right)\tau_{yy}$
τ_{xy}	We	0	$-\dfrac{1}{2}\,We(\tau_{xx}-\tau_{yy})\left(\dfrac{\partial U}{\partial y}-\dfrac{\partial V}{\partial x}\right)+\dfrac{1}{2}\,a\,We(\tau_{xx}+\tau_{yy})\left(\dfrac{\partial U}{\partial y}+\dfrac{\partial V}{\partial x}\right)$ $+w_r\left(\dfrac{\partial U}{\partial y}+\dfrac{\partial V}{\partial x}\right)-\left(1+\varepsilon\,\dfrac{We}{\omega_r}\,\mathrm{Tr}(\underline{\underline{\tau}})\right)\tau_{xy}$

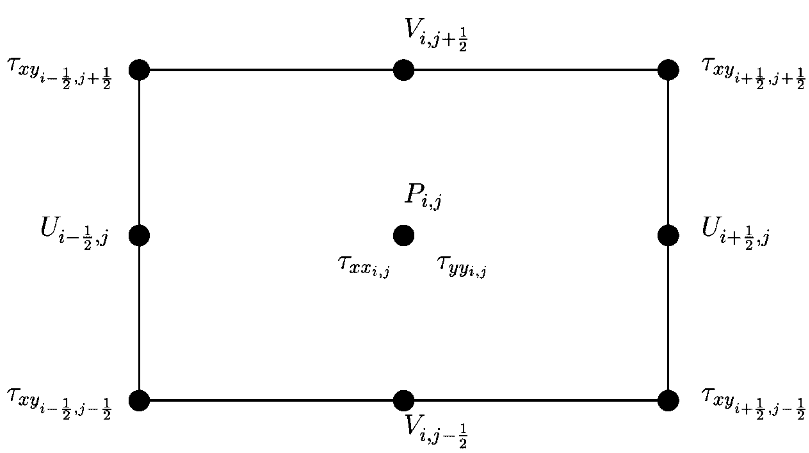

Figure 1. Pressure, velocity and stress tensor in the cell (i, j).

for different equations. For the form of primitive variable, the coefficients Γ and $\wedge$, and source term S_Φ, refer to Table I.

We use a non-uniform staggered grid system. In a staggered grid as shown in Figure 1, pressure P, τ_{xx} and τ_{yy} are cell centred, whereas the components of the velocity are defined at the middle of the sides. The component τ_{xy} of the stress is defined at the top of a cell.

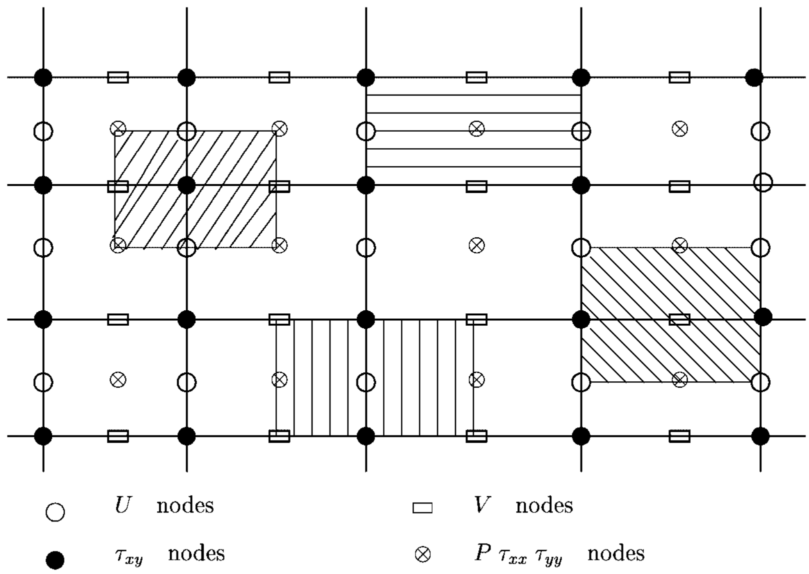

Figure 2. Control volumes for $P, U, V, \tau_{xx}, \tau_{yy}, \tau_{xy}$.

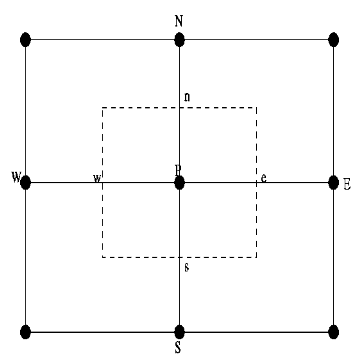

Figure 3. The control volume for grid point P.

The flow domain is divided into a set of non-overlapping control volumes V over which Equation (6) is integrated.

A control volume in two-dimensional space is determined by a quadrilateral surrounding a grid point (see Figures 2–4)

Using the divergence theorem, integration of Equation (6) over the area of a cell leads to the equivalent integral relation

$$\wedge \frac{\mathrm{d}}{\mathrm{d}t} \int_{\text{cell area}} \Phi \,\mathrm{d}x\,\mathrm{d}y + \oint_{\text{cell faces}} \left(\wedge U \Phi - \Gamma \frac{\partial \Phi}{\partial x} \right) \mathrm{d}y - \left(\wedge V \Phi - \Gamma \frac{\partial \Phi}{\partial y} \right) \mathrm{d}x$$
$$= \int_{\text{cell area}} S_\Phi \,\mathrm{d}x\,\mathrm{d}y$$

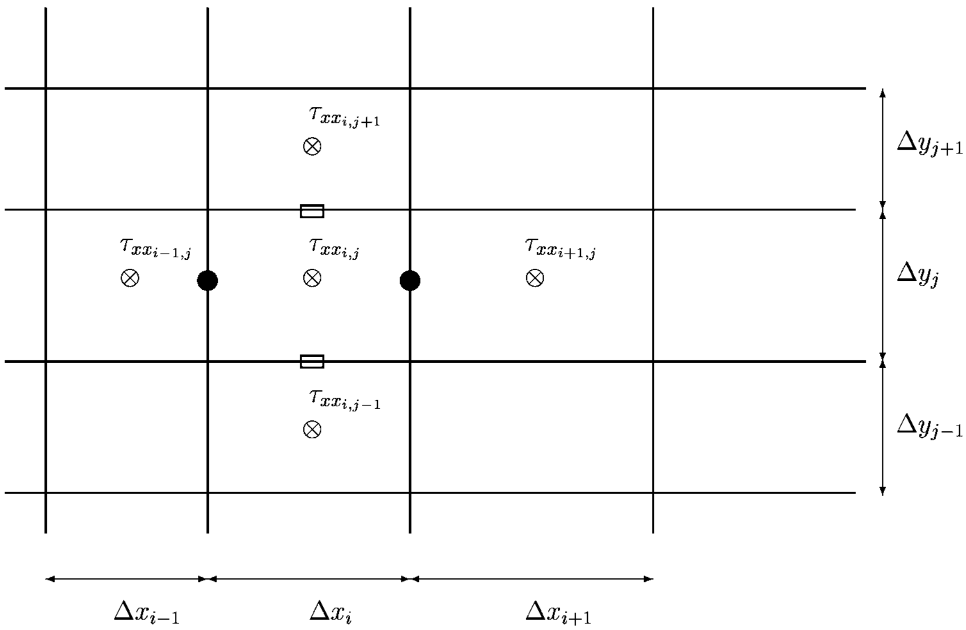

Figure 4. Finite volume discretization for τ_{xx}.

The $(\mathrm{d}/\mathrm{d}t)\int_{\text{cell area}} \Phi\,\mathrm{d}x\,\mathrm{d}y$ term in the above relation represents the change in time of the state primitive variable Φ over the cell area and is discretized, using first-order Euler implicit formula as $(\Delta V/\Delta t)(\Phi_P - \Phi_P^n)$.

ΔV is the control volume magnitude, the subscript P refers to the grid point where the quantity is defined, and the subscript n denotes the value evaluated at time-level n and Δt is a time-step.

The term S_Φ is generally assumed to be a linear function of variable Φ:

$$S_\Phi = S_C + S_P \Phi_P$$

where S_C is the part of S_Φ that does not explicitly depend on Φ and S_P is the coefficient of Φ_P which is made negative to enhance the numerical stability of the discretized equation (see References [30, 24]).

The resulting integrated equation can be expressed symbolically in pseudo-linear form

$$A_P \Phi_P = \sum_I A_I \Phi_I + b_P$$

where the index I runs over the nodal points W, E, N, S (see Figure 3)

$$\int_{\text{cell area}} S_\Phi \,\mathrm{d}x\,\mathrm{d}y = \bar{S}_C + \bar{S}_P \Phi_P$$

$$b_P = \bar{S}_C + A_P^0\, \bar{\Phi}_P^n$$

$$A_P^0 = \wedge\,\frac{\Delta V}{\Delta t}$$

$$A_I = D_i f(|Pe_i|) + \max(\text{sign}(i)F_i, 0)$$
$$A_P = \sum_I A_I - \bar{S}_P + A_P^0$$

where the index i refers to the control volume surfaces ($i \in \{w, e, s, n\}$); D_i is the local diffusion conductance; F_i is the mass flux through the corresponding face normal to i direction of control volume; Pe_i is the local Peclet number defined by $Pe_i = F_i/D_i$; sign(i) is $+1$ for $i \in \{w, s\}$ and -1 for $i \in \{e, n\}$.

An overbar means that the applied values are evaluated using the known fields from the previous time (or iteration) level.

In our calculations, the hybrid scheme is used in the momentum equations:

$$f(|Pe_i|) = \max\left(0, 1 - \frac{|Pe_i|}{2}\right)$$

while upwind scheme is used in the constitutive equations for the stresses:

$$f(|Pe_i|) = 1$$

Consider the discretized form of the τ_{xx} equation ($a = 1$):

$$A_P \tau_{xx_{i,j}} = A_W\, \tau_{xx_{i-1,j}} + A_E \tau_{xx_{i+1,j}} + A_S \tau_{xx_{i,j-1}} + A_N \tau_{xx_{i,j+1}} + b1_{i,j}$$
$$F_e = We\, U_{i+1/2,j} \Delta y_j, \quad F_w = We\, U_{i-1/2,j}\, \Delta y_j$$
$$F_s = We\, V_{i,j-1/2} \Delta x_i, \quad F_n = We\, V_{i,j+1/2} \Delta x_i$$
$$D_e = \Gamma \frac{2\Delta y_j}{\Delta x_i + \Delta x_{i+1}}, \quad D_w = \Gamma \frac{2\Delta y_j}{\Delta x_{i-1} + \Delta x_i}$$
$$D_s = \Gamma \frac{2\Delta x_i}{\Delta y_{j-1} + \Delta y_j}, \quad D_n = \Gamma \frac{2\Delta x_i}{\Delta y_j + \Delta y_{j+1}}$$
$$A_E = D_e + \max(-F_e, 0), \quad A_W = D_w + \max(F_w, 0)$$
$$A_S = D_s + \max(F_s, 0), \quad A_N = D_n + \max(-F_n, 0)$$
$$A_P = A_W + A_E + A_S + A_N + \Delta x_i \Delta y_j + We \frac{\Delta x_i \Delta y_j}{\Delta t} + \varepsilon \frac{We}{\omega_r} (\tau^n_{xx_{i,j}} + \tau^n_{yy_{i,j}}) \Delta x_i \Delta y_j$$
$$b1_{i,j} = 2\, We (U_{i+1/2,j} - U_{i-1/2,j}) \Delta y_j \tau^n_{xx_{i,j}} + 2\omega_r (U_{i+1/2,j} - U_{i-1/2,j}) \Delta y_j$$
$$+ 2\, We (\mathrm{d}U\, \mathrm{d}Y)_{i,j} \tau^n_{xy_{i,j}}\, \Delta x_i \Delta y_j + We \frac{\Delta x_i \Delta y_j}{\Delta t}\, \tau^n_{xx_{i,j}}$$

$(\mathrm{d}U\, \mathrm{d}Y)_{i,j}$ is the discretization of $\partial U/\partial y$ at the grid point P.

The discretized form of the τ_{yy} equation is

$$A_P \tau_{yy_{i,j}} = A_W\, \tau_{yy_{i-1,j}} + A_E \tau_{yy_{i+1,j}} + A_S \tau_{yy_{i,j-1}} + A_N \tau_{yy_{i,j+1}} + b2_{i,j}$$
$$F_e = We\, U_{i+1/2,j} \Delta y_j, \quad F_w = We\, U_{i-1/2,j} \Delta y_j$$
$$F_s = We\, V_{i,j-1/2}\, \Delta x_i, \quad F_n = We\, V_{i,j+1/2} \Delta x_i$$

$$D_e = \Gamma\,\frac{2\Delta y_j}{\Delta x_i + \Delta x_{i+1}}, \quad D_w = \Gamma\,\frac{2\Delta y_j}{\Delta x_{i-1} + \Delta x_i}$$

$$D_s = \Gamma\,\frac{2\Delta x_i}{\Delta y_{j-1} + \Delta y_j}, \quad D_n = \Gamma\,\frac{2\Delta x_i}{\Delta y_j + \Delta y_{j+1}}$$

$$A_E = D_e + \max(-F_e, 0), \quad A_W = D_w + \max(F_w, 0)$$

$$A_S = D_s + \max(F_s, 0), \quad A_N = D_n + \max(-F_n, 0)$$

$$A_P = A_W + A_E + A_S + A_N + \Delta x_i \Delta y_j + We\,\frac{\Delta x_i \Delta y_j}{\Delta t} + \varepsilon\,\frac{We}{\omega_r}(\tau^n_{xx_{i,j}} + \tau^n_{yy_{i,j}})\Delta x_i \Delta y_j$$

$$\begin{aligned} b2_{i,j} = {} & 2\,We(V_{i,j+1/2} - V_{i,j-1/2})\Delta x_i \tau^n_{yy_{i,j}} + 2\omega_r(V_{i,j+1/2,j} - V_{i,j-1/2,j})\Delta x_i \\ & + 2\,We\,(\mathrm{d}V\,\mathrm{d}X)_{i,j}\tau^n_{xy_{i,j}}\Delta x_j \Delta y_j + We\,\frac{\Delta x_i \Delta y_j}{\Delta t}\,\tau^n_{yy_{i,j}} \end{aligned}$$

$(\mathrm{d}V\,\mathrm{d}X)_{i,j}$ is the discretization of $\partial V/\partial x$ at the grid point P.

And for τ_{xy} equation the discretized form is

$$\begin{aligned} A_P \tau_{xy_{i-1/2,j-1/2}} = {} & A_W\,\tau_{xy_{i-3/2,j-1/2}} + A_E \tau_{xy_{i+3/2,j-1/2}} + A_S\,\tau_{xy_{i-1/2,j-3/2}} + A_N\,\tau_{xy_{i-1/2,j+3/2}} \\ & + b3_{i-1/2,j-1/2} \end{aligned}$$

$$F_e = We\,U_{i,j-1/2}\,\frac{(\Delta y_j + \Delta y_{j-1})}{2}, \quad F_w = We\,U_{i-1,j-1/2}\,\frac{(\Delta y_j + \Delta y_{j-1})}{2}$$

$$F_s = We\,V_{i-1/2,j-1}\,\frac{(\Delta x_i + \Delta x_{i-1})}{2}, \quad F_n = We\,V_{i-1/2,j}\,\frac{(\Delta x_i + \Delta x_{i-1})}{2}$$

$$D_e = \Gamma\,\frac{(\Delta y_j + \Delta y_{j-1})}{2\Delta x_i}, \quad D_w = \Gamma\,\frac{(\Delta y_j + \Delta y_{j-1})}{2\Delta x_{i-1}}$$

$$D_s = \Gamma\,\frac{(\Delta x_i + \Delta x_{i-1})}{2\Delta y_{j-1}}, \quad D_n = \Gamma\,\frac{(\Delta x_i + \Delta x_{i-1})}{2\Delta y_j}$$

$$A_E = D_e + \max(-F_e, 0), \quad A_W = D_w + \max(F_w, 0)$$

$$A_S = D_s + \max(F_s, 0), \quad A_N = D_n + \max(-F_n, 0)$$

$$\begin{aligned} A_P = {} & A_W + A_E + A_S + A_N + \frac{(\Delta x_i + \Delta x_{i-1})}{2}\,\frac{(\Delta y_j + \Delta y_{j-1})}{2} \\ & + We\,\frac{(\Delta x_i + \Delta x_{i-1})}{2}\,\frac{(\Delta y_j + \Delta y_{j-1})}{2}\,\frac{1}{\Delta t} \\ & + \varepsilon\,\frac{We}{\omega_r}(\tau^n_{xx_{i,j}} + \tau^n_{yy_{i,j}})\frac{(\Delta x_i + \Delta x_{i-1})}{2}\,\frac{(\Delta y_j + \Delta y_{j-1})}{2} \end{aligned}$$

$$\begin{aligned} b3_{i-1/2,j-1/2} = {} & (V_{i,j-1/2} - V_{i-1,j-1/2})\,\frac{(\Delta y_j + \Delta y_{j-1})}{2}\,(We\,\tau_{xx_{i-1/2,j-1/2}} + \omega_r) \\ & + (U_{i-1/2,j} - U_{i-1/2,j-1})\,\frac{(\Delta x_i + \Delta x_{i-1})}{2}\,(We\,\tau_{yy_{i-1/2,j-1/2}} + \omega_r) \\ & + We\,\frac{(\Delta x_i + \Delta x_{i-1})}{2}\,\frac{(\Delta y_j + \Delta y_{j-1})}{2}\,\frac{1}{\Delta t}\,\tau^n_{xy_{i-1/2,j-1/2}} \end{aligned}$$

where the unknown values $U_{i,j-1/2}, U_{i-1,j-1/2}, V_{i-1/2,j-1}, V_{i-1/2,j}$, $\tau_{xx_{i-1/2,j-1/2}}$ and $\tau_{yy_{i-1/2,j-1/2}}$ are computed by linear interpolation of the four known neighbours.

4. SOLUTION METHOD

To obtain the kinematic fields, the derivation of pressure equation to calculate the pressure field is obviously needed. The semi-implicit method for the pressure linked equation revised (SIMPLER) algorithm of Patankar [30] is used. Detailed procedures of the SIMPLER algorithm have been well documented in the work of Xue *et al.* [27].

The non-linearity of the stress equations used for Oldroyd-B or Phan Thien–Tanner fluids requires the use of iterative schemes to obtain numerical solutions. The approach adopted in this work is to decouple the stress and momentum equations, and to solve each in turn for the stress or velocity field, with the other kept fixed, until a converged state is reached. Thus decoupled approaches reduce the full problem to repeatedly solving two much simpler problems.

The discretized equations for each control volume in the flow domain consist of set of linear algebraic equations that can be solved easily by a generalization of the tridiagonal matrix algorithm (TDMA) algorithm for two dimensions, in combination with a multigrid method. To stabilize the calculations, a global under-relaxation with a factor of 0.7 is used for the velocity component. The stresses are also under-relaxed by a global factor of 0.1.

Because of the implicit nature of the iterative Euler scheme, the time-step Δt is not constrained by the Courant stability limit encountered in explicit schemes. For the range of *We* calculations in this paper, value of $\Delta t = 0.1$ is found to be satisfactory to obtain a stable and converged solution. The convergence criteria is evaluated by requiring that residuals of the discretized equations over all control volumes for any dependent variable is less than the input tolerance, of the order 10^{-6}.

In this work, the predefined level of tolerance to which steady-state convergence is demanded is taken as $\|S^{n+1} - S^n\|/\|S^{n+1}\| < 10^{-6}$ where S^n is the solution vector at time $n\Delta t$, and $\|.\|$ is L_2 measure.

We use continuation techniques to obtain convergent solutions at high Weissenberg number, by increasing the Weissenberg number and the initial condition is taken as the previous *We* solution.

5. MULTIGRID METHOD

To improve the convergence speed of the scheme, we introduce a multigrid method. An efficient multigrid algorithm for solving the resulting discrete equations is developed. Known $(\underline{U}^n, P^n, \underline{\underline{\tau}}^n)$ at time $n\Delta t$, we use a FAS multigrid algorithm (see References [31, 32, 23]) to calculate $(\underline{U}^{n+1}, P^{n+1}, \underline{\underline{\tau}}^{n+1})$ at time $(n+1)\Delta t$.

Let $(\Omega_t)_{1 \leqslant l \leqslant N}$ be a set of N grids of domain Ω, Ω_N is the finest grid and Ω_1 is the coarest grid.

On each grid, we solve

$$L_l(\underline{U}_l, P_l, \underline{\underline{\tau}}_l) = b_l \tag{7}$$

We denote by ε_N the required precision on grid Ω_N, r_l the residual on grid Ω_l, P_l the previous residual on grid Ω_l and η the coefficient of allowed divergence rate.

FAS algorithm

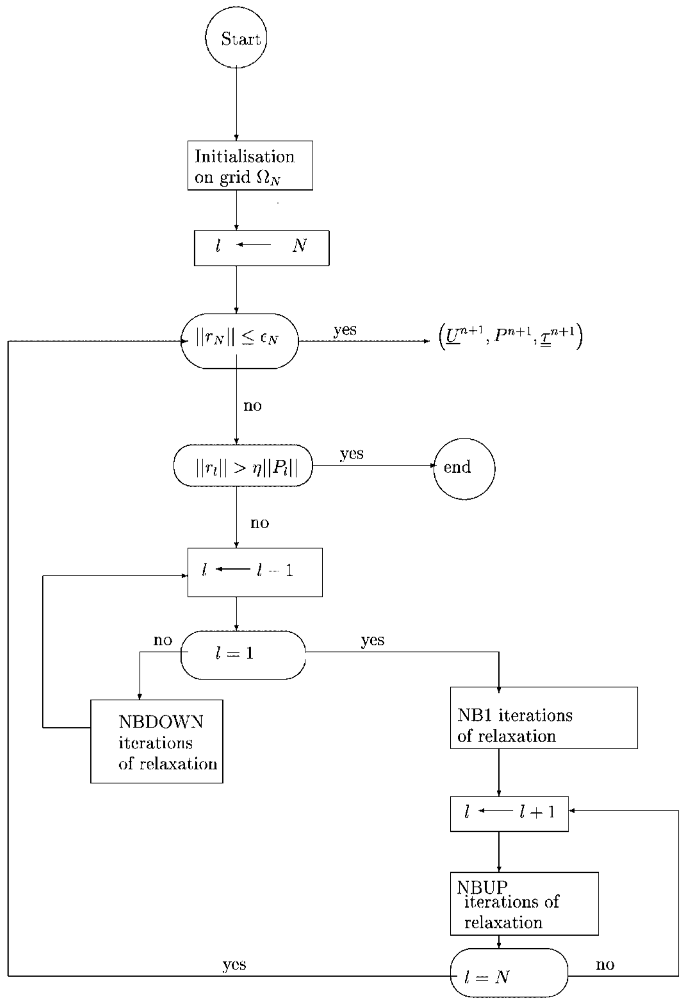

5.1. Resolution on one grid: decoupled formulation

In this section we see how to solve system (7) on each grid Ω_l. This system is obtained by discretizing problem (5) on grid Ω_l.

On each grid Ω_l we decompose system (7) as follows:

$$L_l^1(\underline{U}_l, P_l, \underline{\underline{\tau}}_l) = b_l^1 \tag{8}$$

$$L_l^2(\underline{U}_l, P_l, \underline{\underline{\tau}}_l) = b_l^2 \tag{9}$$

(8) presents the discretization of the momentum and continuity equations, and boundary conditions for $\underline{U}$. The unknown variables are the velocity and pressure. The stress tensor is a known data of problem (8).

(9) presents the discretization of the constitutive equation and the boundary conditions for $\underline{\underline{\tau}}$. The unknown variable is the stress tensor and the velocity field is known.

We execute an m_l iterations in the following method.

Step 1

At the first iteration $\underline{\underline{\tau}}_l$ is initialized on the grid Ω_l, in the following iterations $\underline{\underline{\tau}}_l$ is given by Step 2 of the previous iteration. We take this value of $\underline{\underline{\tau}}_l$ in (8) that we solve by executing a number *itvit* equilibrium and continuity iterations.

Step 2

We take back the values of $\underline{U}_l$ obtained at Step 1 in (9) that we solve by executing a number *itcont* stress tensor iterations.

The numerical experiences have shown that we must choose *itvit* larger than *itcont* to ensure the stability of the method. In numerical tests we have taken $itvit = 5$ or 10 and $itcont = 1$.

6. NUMERICAL RESULTS

The numerical study in this paper is to compute the steady creeping flow of an Oldroyd-B and Phan Thien–Tanner fluids through four-to-one abrupt plane contraction. The flow through a four-to-one abrupt plane contraction is heavily cited in the literature, having been extensively studied numerically [6, 12, 16, 25, 33–36]. This viscoelastic benchmark problem is very difficult to solve. One of the difficulties in treating such a flow is the presence of the re-entrant corner where the stresses become extremely high at higher elasticity resulting in numerical instability and loss of convergence of the solution. Based on the previous numerical results [36], symmetry considerations lead us to consider only half of the geometry. The schematic flow diagram of the computational domain and the boundary conditions are shown in Figure 5.

Fully developed parabolic velocity profile is prescribed at entry and exit sections. No-slip conditions apply on the solid wall. A vanishing tangential traction and normal velocity component together with a vanishing shear stress are imposed on the line of symmetry. Stress components are also imposed at the inlet.

The upstream tube length is 10 and the downstream tube is 30, and are assumed to be adequate for the prescription of fully developed velocity and stress profiles at the inlet and outlet boundaries.

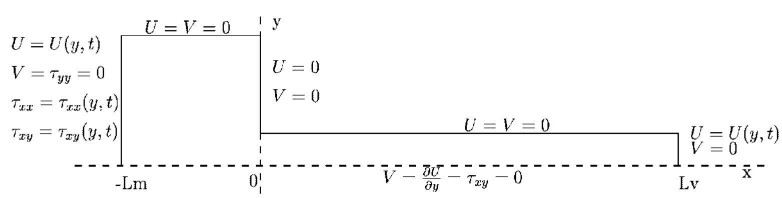

Figure 5. Four-to-one abrupt plane contraction (Lm = 10.0 and Lv = 30.0).

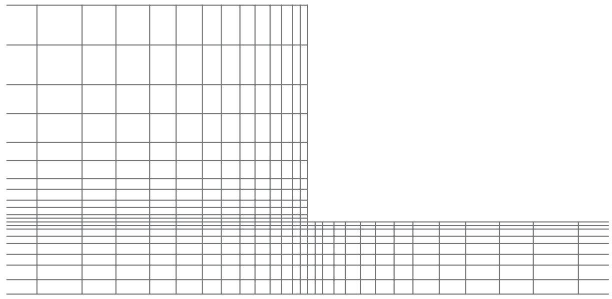

Figure 6. Partial view of the Mesh 2 for the flow in a four-to-one plane contraction (grid Ω_4).

Table II. The CPU reclaimed by four different values of Weissenberg number with both single grid algorithm and FAS algorithm.

CPU	$We=3$	$We=7$	$We=10$	$We=15$
Single grid	1 h 50 mn	2 h 17 mn	7 h 12 mn	10 h 07 mn
FAS algorithm	35 mn	55 mn	1 h 35 mn	2 h 11 mn

One mesh is employed in the present investigation, the Mesh 2 used in Reference [21]. This mesh contains 2624 elements, 17 140 unknown variables and the smallest element at the singularity has a size of $\Delta x=0.05$ and $\Delta y=0.025$. The mesh is depicted in Figure 6.

We have chosen a polymer viscosity ω_r of 0.89, $\varepsilon=0.2$ for Phan Thien–Tanner model and $a=1$ in order to compare our results with the many numerical simulations used to solve this problem. The Reynolds number was set equal to 0.1 for all simulations. For the *We* cases presented in this paper, the computational time required to obtain a converged solution varies approximately from 100 to 200 min of CPU time on a personal computer (PC) with a Pentium processor running at 550 MHz. The calculation is marched until a steady state is reached with full convergence in each time-step.

We wish to examine the smoothness of the solution and the convergence of the method when *We* increases. We have selected on purpose to show the solution profiles on the most difficult portion of the flow boundary, i.e. along the wall near the re-entrant corner and the symmetry line in order to assess the quality of the solutions.

6.1. Oldroyd-B model

First of all we compare the efficiency of the FAS multigrid algorithm with the single-grid algorithm. In Table II we compare for different values of Weisenberg number the time CPU reclaimed by both FAS algorithm and single-grid algorithm. This table shows that if we use the FAS algorithm, we can simulate the 4:1 contraction problem in a short time by using a very thin mesh.

The first velocity component U and the second velocity component V profiles along the line $y=1$ are plotted for $We=10$ in Figure 7. This figure shows an important velocity overshoot. Figure 8 illustrates line plot of first normal stress difference at $We=15.5$ through the

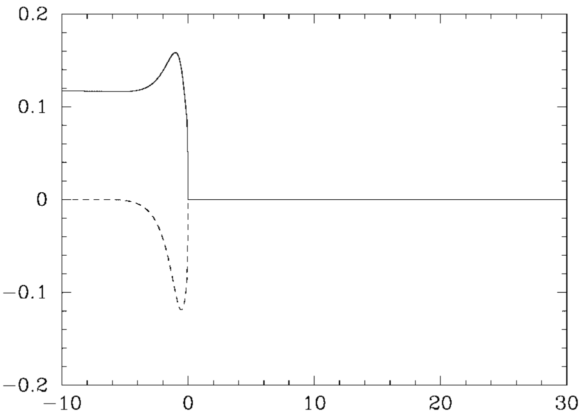

Figure 7. Horizontal and vertical velocity components for the Oldroyd-B model at $We = 10.0$ along the $y = 1$ line.

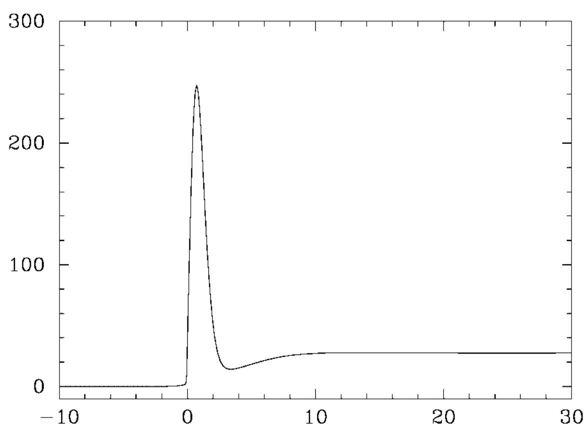

Figure 8. First normal stress difference on $y = 1$ ($We = 15.5$).

re-entrant corner. A high peak is apparent. Figure 9 exhibits the distribution of τ_{xx} along $y = 1$ for three different values of We. Apparently τ_{xx} at the corner causes significant behaviour. As We increases, the values of τ_{xx} at the singular point go up rapidly. The smoothness of the solution is examined by plotting the streamline contours for $We = 10$ as shown in Figure 10. Small recirculation cells may be observed, but no lip vortex. Contours of the τ_{xx} and τ_{xy} shown in Figures 11 and 12, respectively, illustrate physically acceptable state solution for $We = 17$. It is clear that the re-entrant corner represents a strong singularity.

The steady-state solution of the Oldroyd-B model are similar to computed solutions in References [6, 23, 36, 37]. The highest We that we could reach with convergent solutions was 20.

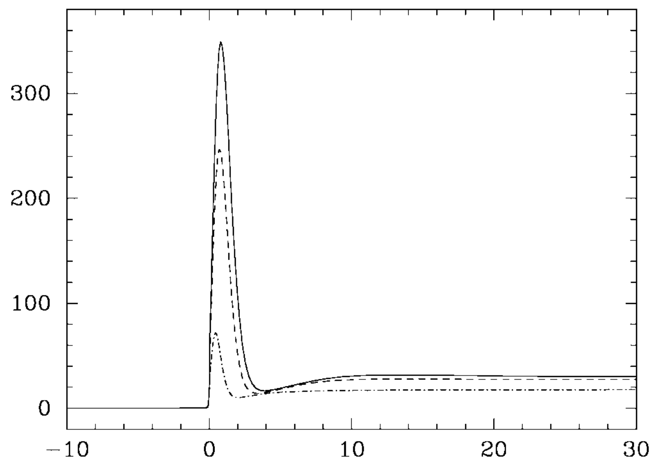

Figure 9. Profiles of τ_{xx} on $y=1$: $We=10$ (-.-.-); $We=15.5$ (- - -); $We=17$(-).

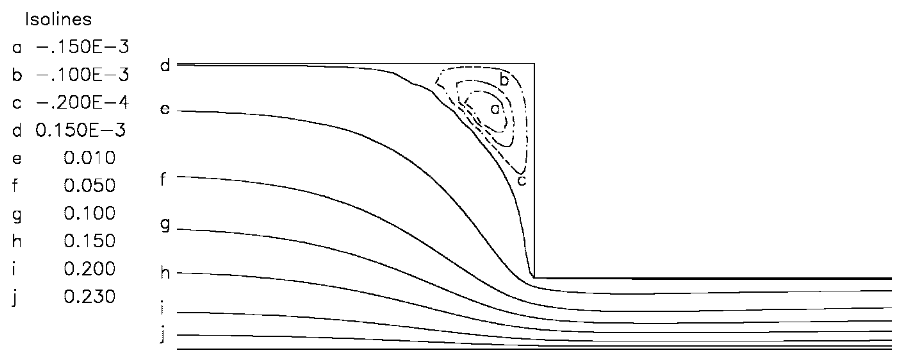

Figure 10. Isolines of streamline function ($We=10$).

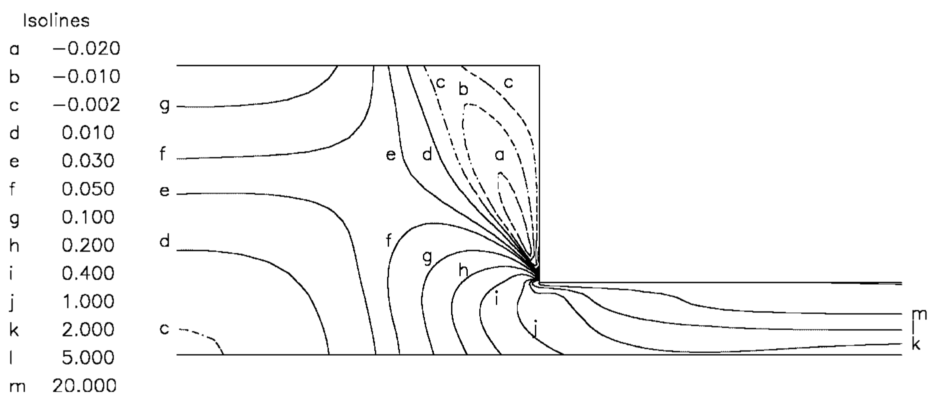

Figure 11. Isolines of τ_{xx} ($We=17$).

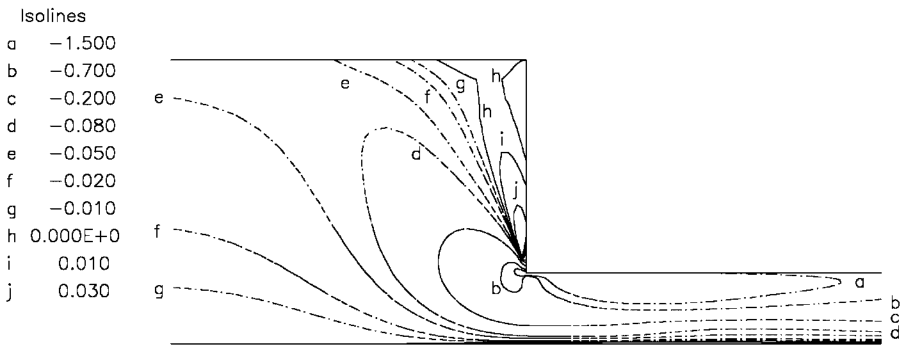

Figure 12. Isolines of τ_{xy} ($We = 17$).

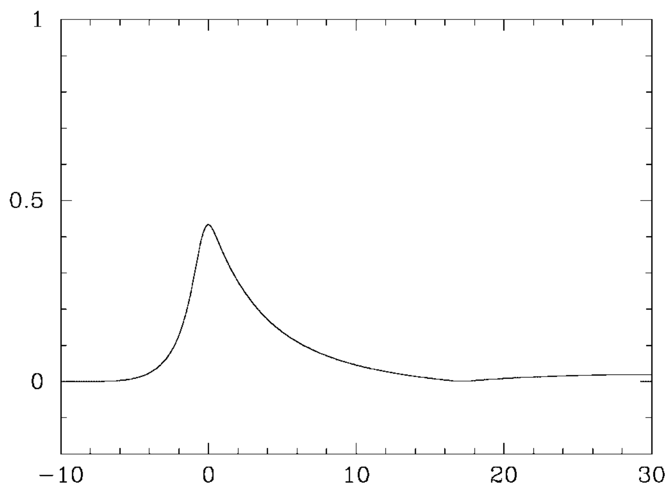

Figure 13. First normal stress difference along the symmetry line ($\varepsilon = 0.2$, $We = 20$).

6.2. Phan Thien–Tanner model

Figure 13 provides the distribution of the normal stress difference $\tau_{xx} - \tau_{yy}$ along the centerline for $We = 20$. It starts from zero upstream in the reservoir, increases to reach a maximum just before the contraction and decreases to become zero. At Weissenberg number of 50, Figure 14 shows the profile of τ_{xx} on a horizontal line through the re-entrant corner. We plot profiles of τ_{yy} and τ_{xy} along the axis $y = 1$, respectively, in Figures 15 and 16. Small singularity observed at the re-entrant corner for the stress tensor. The shape of the peak stress for the Phan Thien–Tanner is similar to the one observed for the Oldroyd-B model but the intensity of the peak differs. The computed streamlines are shown in Figures 17 and 18 for $We = 15$ and 50, respectively. Recirculation zones are formed in the reservoir. Significant changes in vortex activity were observed with increase in We through 15 and 50. The smoothness of the finite volume solutions is further verified by plotting the contours of extra-stress as shown in Figures 19–21 for $We = 20$.

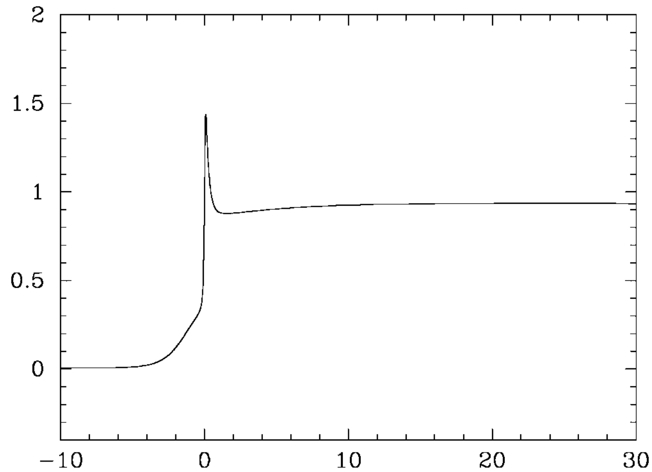

Figure 14. Profile of τ_{xx} on $y = 1$ ($\varepsilon = 0.2$, $We = 50$).

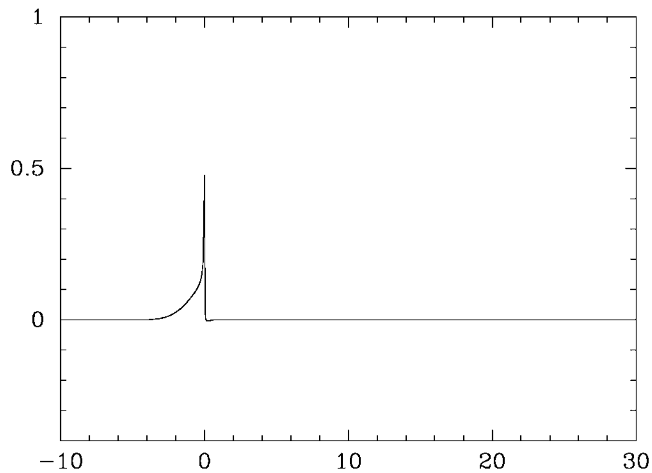

Figure 15. Profile of τ_{yy} on $y = 1$ ($\varepsilon = 0.2$, $We = 50$).

For the Phan Thien–Tanner, calculations are possible up to very high values of We without encountering any loss of convergence for the mesh used.

7. CONCLUSION

A decoupled, implicit finite volume algorithm for solving unsteady viscoelastic flows has been described and implemented for two-dimensional problems. The conservative and constitutive equations are solved using the FVM method on a staggered grid with a hybrid scheme for the velocities and first-order upwind approximation for the viscoelastic stresses. The iterative SIMPLER algorithm is employed to relax the coupled momentum and continuity equations. The

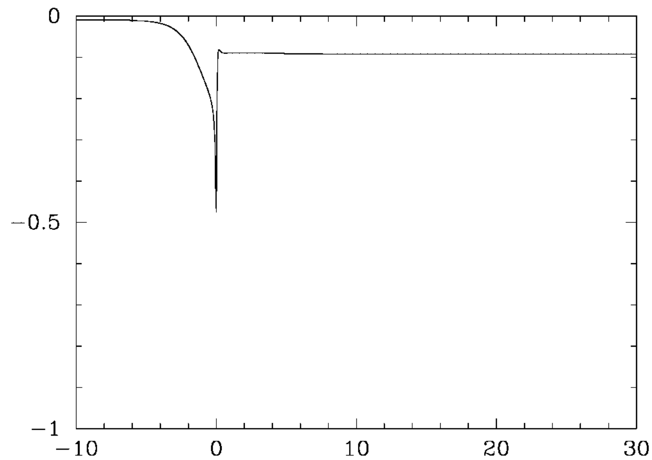

Figure 16. Profile of τ_{xy} on $y=1$ ($\varepsilon=0.2$, $We=50$).

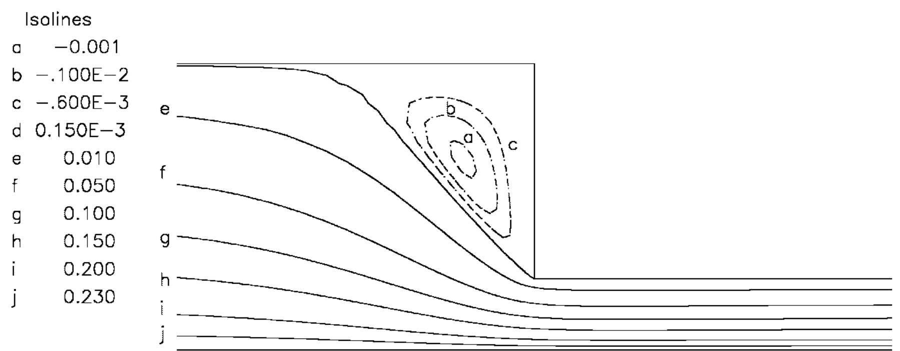

Figure 17. Isolines of streamline function ($\varepsilon=0.2$, $We=15$).

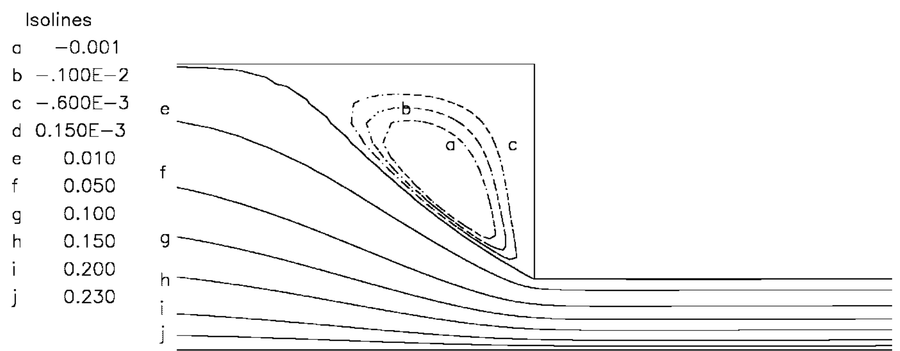

Figure 18. Isolines of streamline function ($\varepsilon=0.2$, $We=50$).

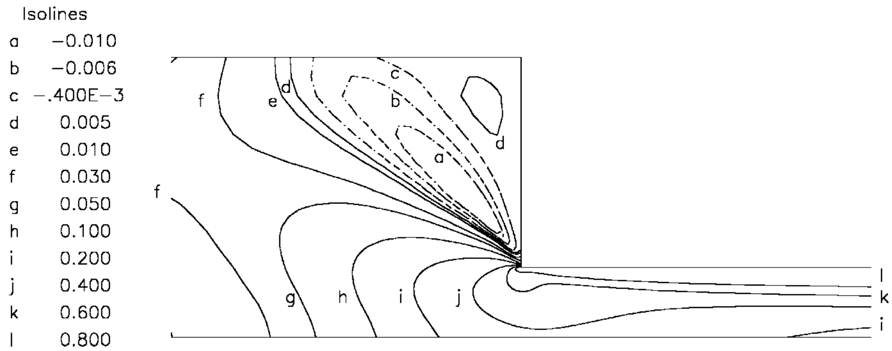

Figure 19. Isolines of τ_{xx} ($\varepsilon = 0.2$, $We = 20$).

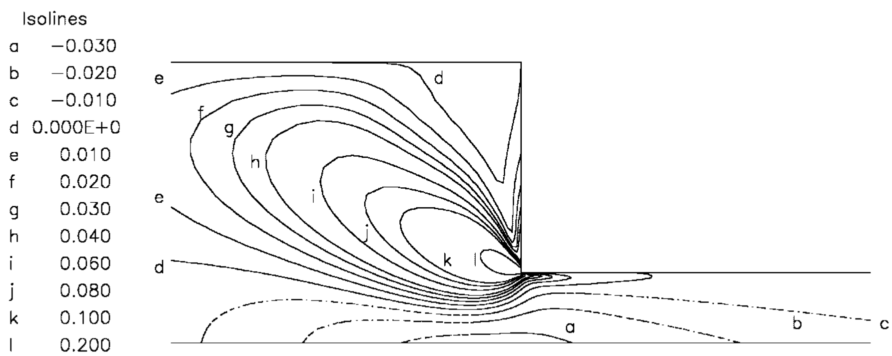

Figure 20. Isolines of τ_{yy} ($\varepsilon = 0.2$, $We = 20$).

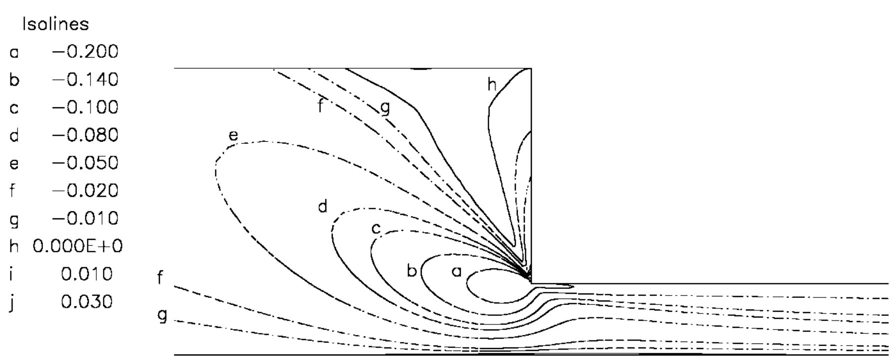

Figure 21. Isolines of τ_{xy} ($\varepsilon = 0.2$, $We = 20$).

discretized equations are solved sequentially, using the TDMA solver with under-relaxation. In both, the FAS multigrid algorithm is used to speed up the convergence rate.

In this study the flows of an Oldroyd-B and Phan Thien–Tanner fluids have been computed in abrupt plane four-to-one contraction. Numerical simulations have been carried out for a wide range of *We* with good convergence of the iterative scheme. For the Oldroyd-B model, we could obtain solutions for *We* as high as 20 and the highest *We* for Phan Thien–Tanner model with $\varepsilon = 0.02$ was 100. No critical Weissenberg number was found when the Phan Thien–Tanner is used with $\varepsilon = 0.2$. The numerical results are satisfactory with regard to computed solutions in the literature. Our simulations have shown that large vortices may be observed when the Weissenberg is high enough. In this paper it was shown that our approach is very efficient and suitable for describing singularity effects. The general features of the method are now to be extended to three-dimensional problems and applied to White–Metzner model.

REFERENCES

1. Tanner RI. In Moldenaers P, Keunings R (eds). *Theoretical and Applied Rheology*, *Proceedings of the XIth International Congress on Rheology*. Brussels, August 1992.
2. Crochet MJ, Davies AR, Walters K. *Numerical Simulation of Non-Newtonian Flow*. Elsevier: Amsterdam, 1984.
3. Armstrong RC, Beris AB, Brown RA, Yeh PW. Galerkin finite element analysis of complex viscoelastic flows. *Computer Methods in Applied Mechanics and Engineering* 1986, **58**:202–226.
4. Brooks AN, Hughes TIR. Streamline upwind/Petrov–Galerkin formulations for convection dominated flows with particular emphasis on the incompressible Navier–Stokes equation. *Computer Methods in Applied Mechanics and Engineering* 1982; **32**:199–259.
5. Joseph DD, Renardy M, Saut JC. Hyperbolicity and change of type in the flow of viscoelastic fluids. *Archives for Rational Mechanics and Analysis* 1985; **87**:213–251.
6. Marchal JM, Crochet MJ. A new mixed finite element for calculation of viscoelastic flow. *Journal of Non-Newtonian Fluid Mechanics* 1987; **26**:77–114.
7. King RC, Apelian MR, Armstrong RC, Brown RA. Numerically stable finite element techniques for viscoelastic calculation in smooth singular geometries. *Journal of Non-Newtonian Fluid Mechanics* 1988; **29**:147–216.
8. Rajagopalan D, Armstrong RC, Brown RA. Finite elements methods for calculation of steady viscoelastic flow using constitutive equations with a Newtonian viscosity. *Journal of Non-Newtonian Fluid Mechanics* 1990; **36**:159–192
9. Rao RR, Finlayson BA. Adaptive refinement of viscoelastic flow problem with the explicitly elliptic momentum equations. *Journal of Non-Newtonian Fluid Mechanics* 1991; **38**:223–246.
10. Rao RR, Finlayson BA. Viscoelastic flow simulation using cubic stress finite elements. *Journal of Non-Newtonian Fluid Mechanics* 1992; **43**:61–82.
11. Fortin M, Fortin A. A preconditioned gmres algorithm for the numerical solution of viscoelastic fluid flows. *Journal of Non-Newtonian Fluid Mechanics* 1990; **36**:277–288.
12. Fortin M, Fortin A. A new approach for the fem simulation of viscoelastic flows. *Journal of Non-Newtonian Fluid Mechanics* 1989; **32**:295–310.
13. Fortin A, Zine A. An improved gmres method for solving viscoelastic fluid flow problems. *Journal of Non-Newtonian Fluid Mechanics* 1992; **42**:1–18.
14. Armstrong RC, Beris AB, Brown RA. Spectral/finite element calculations of the flow of a Maxwell fluid between eccentric rotating cylinders. *Journal of Non-Newtonian Fluid Mechanics* 1987; **22**:129.
15. Talwar KK, Khomami B, Ganpule HK. A comparative study of higher and lower order finite element techniques for computation of viscoelastic flows. *Journal of Rheology* 1994; **38**:255–289.
16. Carew EO, Townsend P, Webster MF. A Taylor Petrov–Galerkin algorithm for viscoelastic flow. *Journal of Non-Newtonian Fluid Mechanics* 1993; **50**:253–287.
17. Keiller RA. Entry-flow calculations for the Oldroyd-B and fene equations. *Journal of Non-Newtonian Fluid Mechanics* 1993; **46**:143–178.
18. Choi HC, Song JH, Yoo JY. Numerical simulation of the planar contraction flow of a Gieskus fluid. *Journal of Non-Newtonian Fluid Mechanics* 1988; **29**:347–379.
19. Gasti TB. Steady flow of a non-Newtonian fluid through a contraction. *Journal of Computational Physics* 1975; **27**:42–70.
20. Al Moatassime H, Jouron C. A multigrid method for solving steady viscoelastic fluid flow. *Computer Methods in Applied Mechanics and Engineering* 2001; **190/31**:4061–4080.
21. Al Moatassime H, Esselaoui D. A new efficient solver for steady viscoelastic fluid flow problem. *Proceedings of the International Conference on Numerical Algorithms, Marrakech, Morocco, 1–5 October 2001*.
22. Darwish MS, Whiteman JR, Bevis MJ. Numerical modelling of viscoelastic liquids using a finite volume method. *Journal of Non-Newtonian Fluid Mechanics* 1992; **45**:311–337.
23. Al Moatassime H, Esselaoui D, Hakim A, Raghay S. Finite volume multigrid method of the planar contraction flow of a viscoelastic fluid. *International Journal of Numerical methods in Fluids* 2001; **36**:885–902.

24. Sasmal GP. Finite volume approach for calculation of viscoelastic flow through an abrupt axisymmetric contraction. *Journal of Non-Newtonian Fluid Mechanics* 1995; **56**:15–47.
25. Yoo JY, Na Y. A numerical study of the planar contraction flow of a viscoelastic fluid using the simpler algorithm. *Journal of Non-Newtonian Fluid Mechanics* 1991; **39**:89–106.
26. Luo XL. A control volume approach for integral viscoelastic models and its application to contraction flow of polymer melts. *Journal of Non-Newtonian Fluid Mechanics* 1996; **64**:173–189.
27. Xue SC, Phan–Thien N, Tanner RI. Numerical study of secondary flows of viscoelastic fluid in straight pipes by an implicit finite volume method. *Journal of Non-Newtonian Fluid Mechanics* 1995; **59**:191–213.
28. Tanner RI. Constitutive model for VIIth Workshop on numerical computations in viscoelastic flows. Personal Communication, 1989.
29. Phan–Thien N, Tanner RI. A new constitutive equation derived from network theory. *Journal of Non-Newtonian Fluid Mechanics* 1977; **2**:353.
30. Patankar SV. *Numerical Heat Transfer and Fluid Flow*. Hemisphere: New York, 1980.
31. Brandt A. Multilevel adaptive solutions to boundary value problems. *Mathematical Computations* 1987; **31**: 333–390.
32. Hackbusch W. *Multi-Grid Methods and Applications*. Springer: Berlin, 1985.
33. Fortin M, Esselaoui D. Finite element procedure for viscoelastic flows. *International Journal for Numerical Methods in Engineering* 1987; **7**:1035–1052.
34. Marchal JM, Crochet MJ. Hermetian finite elements for calculating viscoelastic flow. *Journal of Non-Newtonian Fluid Mechanics* 1986; **20**:187–207.
35. Keunings R. On the high Weissenberg number problem. *Journal of Non-Newtonian Fluid Mechanics* 1986; **20**:209–226.
36. Marduel X. Simulations numériques de fluides viscoélastiques, *Ph.D. Thesis*, Université Paris XI Orsay, 1997.
37. Maders H. Une moddélisation par éléments finis de l'écoulement d'un fluide viscoélastique dans unde filière idimensionnelle. *Ph.D. Thesis*, Ecole Nationale Supérieure des Mines de Paris, 1990.

